AIP | Applied Physics Letters

Voltage-tunable terahertz and infrared photodetectors based on double-graphene-layer structures

V. Ryzhii, T. Otsuji, V. Ya. Aleshkin, A. A. Dubinov, M. Ryzhii, V. Mitin, and M. S. Shur

Citation: Applied Physics Letters **104**, 163505 (2014); doi: 10.1063/1.4873114
View online: http://dx.doi.org/10.1063/1.4873114
View Table of Contents: http://scitation.aip.org/content/aip/journal/apl/104/16?ver=pdfcov
Published by the AIP Publishing

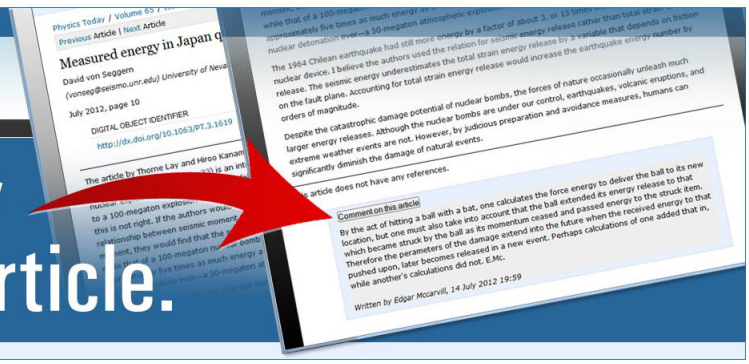

Voltage-tunable terahertz and infrared photodetectors based on double-graphene-layer structures

V. Ryzhii,[1,2,a)] T. Otsuji,[1] V. Ya. Aleshkin,[3] A. A. Dubinov,[3] M. Ryzhii,[4] V. Mitin,[5] and M. S. Shur[6]

[1]*Research Institute for Electrical Communication, Tohoku University, Sendai 980-8577, Japan*
[2]*Institute of Ultra High Frequency Semiconductor Electronics, Russian Academy of Sciences, Moscow 111005, Russia*
[3]*Institute for Physics of Microstructures of Russian Academy of Sciences, and Lobachevsky State University of Nizhny Novgorod, Nizhny Novgorod 603950, Russia*
[4]*Department of Computer Science and Engineering, University of Aizu, Aizu-Wakamatsu 965-8580, Japan*
[5]*Department of Electrical Engineering, University at Buffalo, Buffalo, New York 1460-1920, USA*
[6]*Department of Electrical, Electronics, and System Engineering, Rensselaer Polytechnic Institute, Troy, New York 12180, USA*

(Received 27 February 2014; accepted 11 April 2014; published online 24 April 2014)

We propose and theoretically substantiate the concept of terahertz and infrared photodetectors using the resonant radiative transitions between graphene layers (GLs) in double-GL structures. The calculated absorption spectrum and the spectral characteristics of the photodetector responsivity exhibit sharp resonant maxima at the photon energies in a wide range. The resonant maxima can be tuned by the applied voltage. We compare the photodetector responsivity with that of the GL p-i-n photodiodes and quantum-well infrared photodetectors. Weak temperature dependences of the photocurrent and dark current enable the effective operation of the proposed photodetector at room temperature. © *2014 AIP Publishing LLC*. [http://dx.doi.org/10.1063/1.4873114]

Fabrication and exploration of double-graphene-layer (double-GL) structures with narrow inter-GL barrier Boron Nitride (bBN), Tungsten Disulfide (WS_2), and other barrier layers[1–4] have recently attracted much attention due to their potential applications in high speed modulators of terahertz (THz) and infrared (IR) radiation,[1,5] transistors,[3] THz photomixers,[6] and lasers.[7,8] The THz lasing in the latter devices is due to the inter-GL population inversion and the inter-GL resonant radiative transitions. The double-GL-based lasers might exhibit advantages over the THz lasers exploiting the intra-GL interband population inversion and vertical radiative transitions[9–14] (see also Refs. 15–18). The nonlinearity of the inter-GL tunneling current in the double-GL structures[3,4,19,20] can also be used for the detection of THz radiation.[21,22] Various graphene-based structures are attractive for the interband THz and IR photodetectors.[18,23–33] In this paper, we propose and evaluate THz/IR photodetectors based on the double-GL structures using the inter-GL resonant optical absorption.

The double-GL photodetectors (DGL-PDs) can exhibit some advantages over the GL-based photodetectors using the intra-GL interband transitions. These advantages are: (1) resonant voltage-tunable spectrum and (2) lower dark current (due to its non-resonant tunneling nature). The latter property should result in large detectivity, particularly, at elevated (room) temperatures. The DGL-PDs under consideration can also find applications in the frequency range between 6 and 10 THz (corresponding to the photon energies $\hbar\omega \simeq 25 - 40$ meV and to the wavelength $\lambda = 30 - 50$ μm), which includes the optical phonon frequencies in A_3B_5 materials and not accessible for such photodetectors as quantum-well and quantum-dot infrared photodetectors (QWIPs and QDIPs)[34,35] due to high absorption by optical phonons.

We consider the DGL-PD structure shown in Fig. 1. The structure in Fig. 1 consists of two independently contacted GLs in which the electrons and holes are induced by the voltages $\pm V_g/2$ applied to the highly conducting gates ("electrical" doping). The top electrode is a grated structure with the grating providing coupling to the incident THz or IR radiation. The bottom gate can serve not only as the gate controlling the carrier density but also as the reflector of the incident radiation. The bias voltage V is applied between the pertinent contacts. These structures are similar to those recently frabricated.[1–4] The grating is necessary because the inter-GL radiative transitions are associated with the component of the radiation electric field perpendicular to the GL plane as in n-type QWIPs (other methods of the radiation

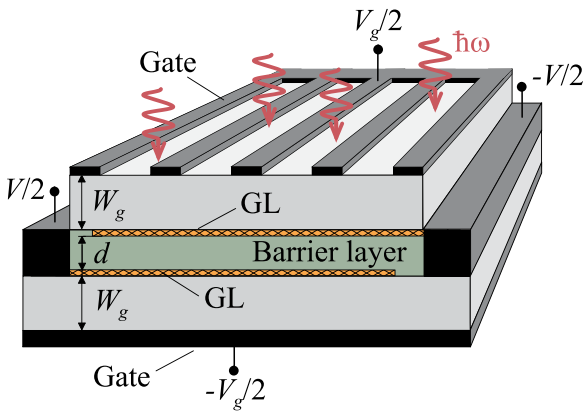

FIG. 1. Schematic view of DGL-PD structure with "electrical doping" and top gate serving as the grating coupler.

[a)]Electronic mail: v-ryzhii(at)riec.tohoku.ac.jp

coupling can be used as well). The DGL-PDs can also use the chemically doped GLs with or without gates.

Under operation conditions, the top GL (n-type GL) is filled the two-dimensional electron gas, while the bottom GL (p-type GL) is filled with the two-dimensional hole gas. The energy gap between the Dirac points in GLs is equal to

$$\frac{\Delta}{e} = V + V_0 - \sqrt{2VV_0 + V_0^2 + V_t^2}, \tag{1}$$

where $V_0 = \hbar^2 v_W^2 \kappa / 2e^3 d$, $V_t = 2\hbar\, v_W \sqrt{\pi \Sigma_i}/e$, $\Sigma_i \propto V_g / W_g$, is the electron and hole densities induced by the gate voltages (or the densities of donors and acceptors in DGL-PDs with the chemical doping), d and W_g are the thicknesses of the barrier and gate layers, respectively (see Fig. 1), κ is the dielectric constant, $e = |e|$ is the electron charge, $\hbar$ is the Planck constant, and $v_W \simeq 10^8$ cm/s is the characteristic velocity of electrons and holes in GLs. Assuming $\kappa = 4$, $d = 4$ nm, and $\Sigma_i = 10^{12}\,\text{cm}^{-2}$, one obtains $V_0 \simeq 136$ mV and $V_t \simeq 221$ mV. Figure 2 shows the band diagrams at $V = 0$ and $0 < V < V_t$. If $V = 0$, the Fermi levels in GLs are flat [see Fig. 2(a)] and $\Delta = -(\mu_e + \mu_h) = -2\mu$, where $\mu_e = \mu_h = \mu$ are the electron and hole Fermi energies at $V = 0$, respectively. At $V \le V_t$, Eq. (1) yields $\Delta \le 0$.

The operation of DGL-PDs is associated with the absorption of the incident IR radiation accompanied by the electron tunneling transitions between GLs and causing the electric terminal current. The inter-GL radiative transitions with the absorption of photons (shown schematically in Fig. 2) with the energy $\hbar\omega$ conserve the electron lateral momentum and, hence, do not involve scattering (resonant-tunneling photon-assisted transitions), if

$$\hbar\omega \simeq -\Delta + \hbar\omega_{dep} = \hbar\omega_{max}. \tag{2}$$

Here,

$$\hbar\omega_{dep} = \frac{8\pi e^2 |z_{u,l}|^2}{\kappa d}\left(\Sigma_i + \frac{\kappa\Delta}{4\pi e^2 d}\right) \tag{3}$$

is the depolarization shift (see, for example, Refs. 36 and 37), $z_{u,l} = \int \varphi_u^*(z) z \varphi_l(z) dz$ is the matrix element of the inter-GL transitions, where $\varphi_u(z)$ and $\varphi_l(z)$ are the z-dependent factors of the wave functions in the upper and lower GLs, respectively (the axis z is directed perpendicular to the GL plane).

The real part of the double-GL structure dynamic conductivity in the direction perpendicular to the GL plane $\sigma_{zz}(\omega)$ can be presented as (compare with Refs. 7 and 8)

$$\text{Re}\sigma_{zz}(\omega) = \left(\frac{e^2}{\hbar}\right)\frac{2|z_{u,l}|^2 \gamma\hbar\omega}{[\hbar^2(\omega - \omega_{max})^2 + \gamma^2]}\left(\Sigma_i + \frac{\kappa\Delta}{4\pi e^2 d}\right). \tag{4}$$

Here, $\gamma \simeq \hbar\nu$ is the relaxation broadening and ν is the collision frequency of electrons and holes. Equation (4) accounts for the transitions both between the conduction and valence band states. The quantity $\hbar\omega_{max}$ in Eq. (4) corresponds to the maximum probability of the inter-GL radiative transitions. In contrast to the double-GL-based devices considered in Refs. 7 and 8, the doping level of GL Σ_i and the bias voltage V are chosen in such a way that $-\Delta + \hbar\omega_{dep} > 0$.

According to Eq. (4), the probability of the inter-GL transition with the absorption of an incident photon with the energy $\hbar\omega$ is given by

$$\beta_\omega = \left(\frac{\pi e^2}{c\hbar}\right)\frac{8|z_{u,l}|^2 \gamma\hbar\omega}{[\hbar^2(\omega - \omega_{max})^2 + \gamma^2]}\left(\Sigma_i + \frac{\kappa\Delta}{4\pi e^2 d}\right)\theta. \tag{5}$$

Here, $\theta < 1$ is the input efficiency (determined by the properties of the grating, reflection, and so on). This yields the following spectral dependence of the DGL-PD responsivity:

$$R_\omega = \left(\frac{\pi e^2}{c\hbar}\right)\frac{8e|z_{u,l}|^2 \gamma}{[\hbar^2(\omega - \omega_{max})^2 + \gamma^2]}\left(\Sigma_i + \frac{\kappa\Delta}{4\pi e^2 d}\right)\theta. \tag{6}$$

Using Eqs. (3) and (6), the maximum of the DGL-PD responsivity, which is achieved at $\hbar\omega = \hbar\omega_{max}$, can be presented as

$$R_{\omega_{max}} = \left(\frac{e\kappa d}{c\hbar}\right)\left(\frac{\hbar\omega_{dep}}{\gamma}\right)\theta. \tag{7}$$

Figure 3 shows the DGL-PD responsivity R_ω versus the photon energy $\hbar\omega$ calculated for different voltages V using Eq. (6) with Δ and $\hbar\omega_{max}$ given by Eqs. (1) and (2), respectively. The parameters used in the calculations were $\kappa = 4$, $\gamma = 1$ meV (i.e., $\nu = 1.6 \times 10^{12}\,\text{s}^{-1}$), $\Sigma_i = 10^{12}\,\text{cm}^{-2}$, $d = 2$ and 4 nm, ($V_0 = 136 - 272$ mV and $V_t = 221$ mV), and $\theta = 0.5$. The quantity $|z_{u,l}|^2$ was calculated for different

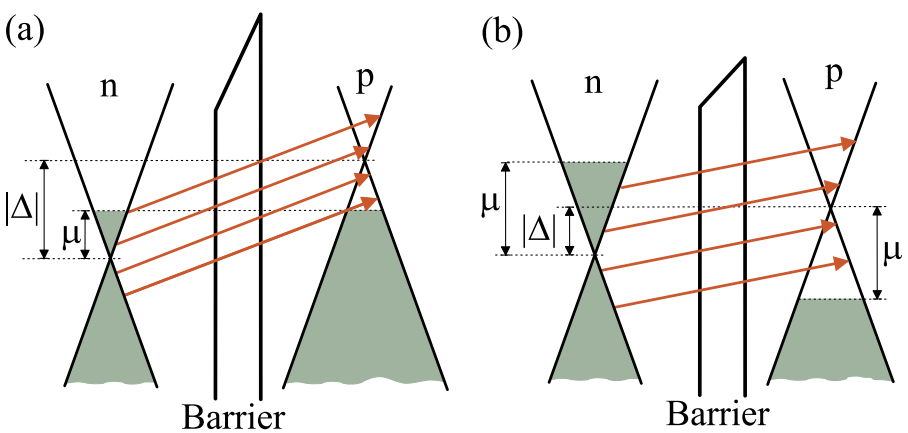

FIG. 2. DGL-PD band diagrams at (a) $V = 0$ and (b) $0 < V < V_t$. Arrows schematically indicate the photon-assisted inter-GL resonant-tunneling transitions between the initial (in n-type GL) and final states (in p-type GL) in the conduction bands and between such states in the valence bands in GLs.

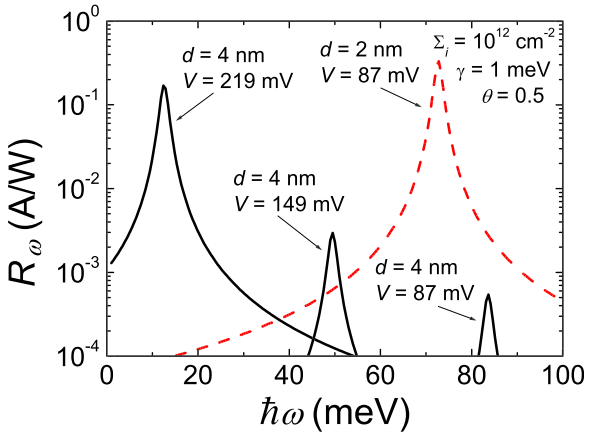

FIG. 3. Dependences of DGL-PD responsivity R_ω on photon energy $\hbar\omega$ for the inter-GL barrier layer thickness $d = 4$ nm (solid lines) and $d = 2$ nm (dashed line) at different applied voltages V.

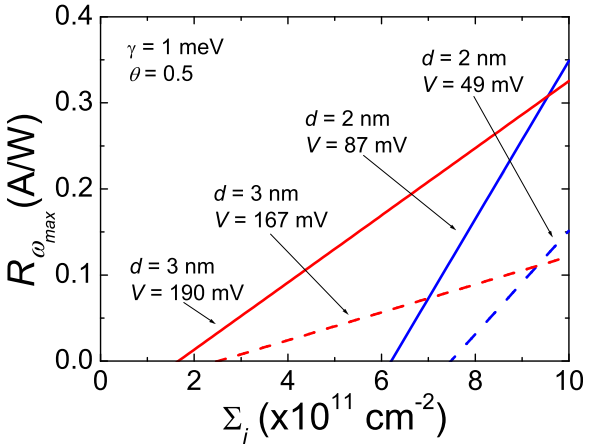

FIG. 5. Dependence of the responsivity maximum $R_{\omega_{max}}$ on the electron and hole density $\Sigma_i \propto V_g/W_g$ at different bias voltages V and thicknesses d.

inter-GL barrier layer (WS_2) thicknesses d as in Refs. 7, 8, and 38. As seen from Fig. 3, the DGL-PD responsivity exhibits fairly sharp peaks associated with the inter-GL resonant-tunneling transitions accompanied by the absorption of the incident photons. The peak values of the responsivity are rather high in a wide spectral range.

Figure 4 shows the dependences of $\hbar\omega_{max}$ and $R_{\omega_{max}}$ on the applied voltage V calculated for different thicknesses, d, of the inter-GL barrier layer. A marked shift of the responsivity maxima with varying bias voltage V (see Figs. 3 and 4) enables the DGL-PD spectrum voltage tuning. However, the height of the responsivity maxima is very sensitive to the bias voltage V (compare peaks for $d = 4$ nm in Fig. 3). This is also seen in Fig. 4. The maximum value of the DGL-PD responsivity markedly depends on the electrical doping determined by the gate voltage V_g (see Fig. 5).

For comparison, the responsivities of a single-GL p-i-n-PD and QWIPs are as follows:[27,34,35]

$$R_\omega^{pin} \simeq \left(\frac{\pi e^2}{c\hbar}\right)\frac{e g^{pin}}{\hbar\omega}, \quad R_\omega^{qwip} \simeq \left(\frac{e}{\hbar\omega}\right)\sigma_i \Sigma_i\, g^{qwip}\theta, \qquad (8)$$

where g^{pin} and g^{qwip} are the GL p-i-n-PD and QWIP photoelectric gains, respectively, and σ_i is the QW photoionization cross-section by an incident photon (with the energy close to the gap between the edge of the QW and the subband bottom). In the DGL-PDs with relatively short i-region with the length of this region shorter than the electron and hole bipolar diffusion length l_D, one obtains $g^{pin} \lesssim 2$. But in the DGL-PDs with a long i-region, $g^{pin} \sim (l_D/l)^2 \ll 1$. The QWIP photoelectric gain g^{qwip} is approximately equal to the probability of the capture of the electron crossing the QW ($g^{qwip} \geq 1$).

Thus, at $\omega = \omega_{max}$, from Eqs. (7) and (8), we obtain

$$\frac{R_{\omega_{max}}}{R^{pin}_{\omega_{max}}} \simeq \frac{\hbar^2\omega_{max}\omega_{dep}\theta}{\varepsilon_d \gamma\, g^{pin}}, \quad \frac{R_{\omega_{max}}}{R^{qwip}_{\omega_{max}}} \simeq \frac{\hbar^2\omega_{max}\omega_{dep}}{\varepsilon_i \gamma\, g^{qwip}}. \qquad (9)$$

Here, $\varepsilon_d = 2\pi e^2/\kappa d$ and $\varepsilon_i = c\hbar\sigma_i\Sigma_i/\kappa d$.

Using the above formulas and assuming $\Sigma_i = 10^{12}\,\text{cm}^{-2}$, $\sigma_i \sim 2 \times 10^{-15}\,\text{cm}^{-2}$,[39] $d = 2$ nm, and $\hbar\omega = 72$ meV at which $R_\omega = 0.3$ A/W (see Fig. 3), one obtains $R_{\omega_{max}}/R^{pin}_{\omega_{max}} \sim \theta/g^{pin}$ and $R_{\omega_{max}}/R^{qwip}_{\omega_{max}} \sim 20/g^{qwip}$. This shows that the peak responsivity of GBL-PDs can exceed that of GL p-i-n-PDs and QWIPs with a moderate photoelectric gain. Figure 6 shows the ratio of the responsivities of DGL-PDs and QWIPs (with $g^{qwip} = 1$) versus the photon energy at which the responsivity achieves the maxima calculated for different doping levels and the inter-GL barrier layer thicknesses.

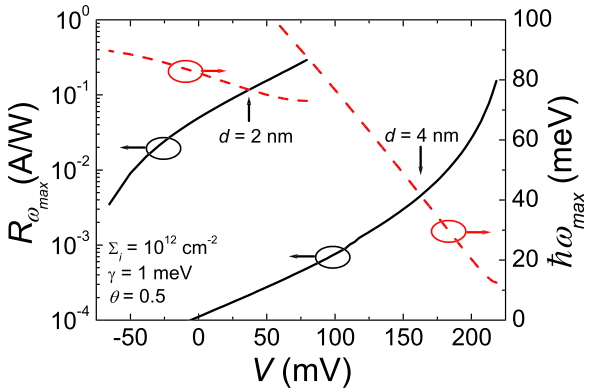

FIG. 4. Dependences of the responsivity maximum $R_{\omega_{max}}$ (solid lines) and corresponding photon energy $\hbar\omega_{max}$ (dashed lines) on bias voltages V for different thicknesses d.

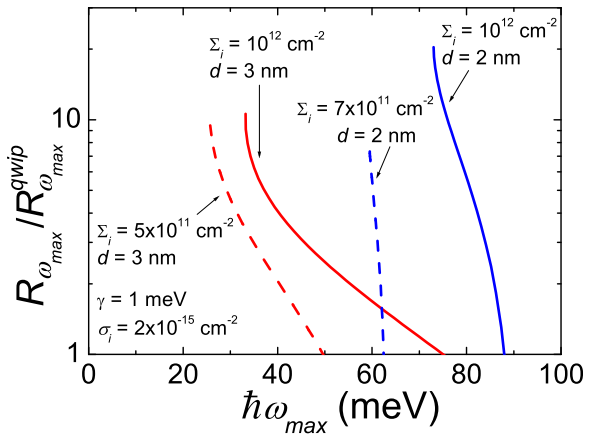

FIG. 6. Ratio of DGL-PD and QWIP responsivities $R_{\omega_{max}}/R^{qwip}_{\omega_{max}}$ versus $\hbar\omega_{max}$ for different Σ_i and d.

Since the dark current in DGL-PDs is associated with the inter-GL tunneling,[2,3] at elevated temperatures it can be much smaller than the dark current in GL p-i-n-PDs.[27] This and a weak temperature dependence of the responsivity are beneficial for achieving high values of the detectivity at elevated temperatures, including the room temperature. However, at the voltage corresponding to $\Delta = 0$, the inter-GL transitions become of the resonant-tunneling origin,[3,19,20] and the dark current in DGL-PDs can exhibit a pronounced peak.

The grating gate period and the gate layer thickness should be optimized to maximize the radiation coupling and limit the spatial periodicity of the carrier (electron) density in the top GL. This periodicity might add more complexity to the DGL-PD spectral characteristics (see, for example, Ref. 40). The pertinent effects require a separate treatment.

In conclusion, we evaluated the responsivity of the proposed DGL-PDs and demonstrated that the DGL-PD responsivity as a function of the photon energy can exhibit the voltage tunable resonant maxima in a wide spectral range. This provides the possibility of implementing of effective DGL-PDs competitive with other THz and IR photodetectors, especially at elevated (room) temperatures.

This work was supported by the Japan Society for Promotion of Science (Grant-in-Aid for Specially Promoting Research, No. 2300000), Japan, and by the Dynasty Foundation, Russia. The works at UB and RPI were supported by the NSF-TERANO Program and the U.S. Army Cooperative Research Agreement (Project Manager Dr. Meredith Reed), respectively.

[1]M. Liu, X. Yin, and X. Zhang, Nano Lett. **12**, 1482 (2012).
[2]L. Britnell, R. V. Gorbachev, R. Jalil, B. D. Belle, F. Shedin, A. Mishenko, T. Georgiou, M. I. Katsnelson, L. Eaves, S. V. Morozov, N. M. R. Peres, J. Leist, A. K. Geim, K. S. Novoselov, and L. A. Ponomarenko, Science **335**, 947 (2012).
[3]T. Georgiou, R. Jalil, B. D. Bellee, L. Britnell, R. V. Gorbachev, S. V. Morozov, Y.-J. Kim, A. Cholinia, S. J. Haigh, O. Makarovsky, L. Eaves, L. A. Ponomarenko, A. K. Geim, K. S. Novoselov, and A. Mishchenko, Nat. Nanotechnol. **8**, 100 (2013).
[4]L. Britnell, R. V. Gorbachev, A. K. Geim, L. A. Ponomarenko, A. Mishchenko, M. T. Greenaway, T. M. Fromhold, K. S. Novoselov, and L. Eaves, Nat. Commun. **4**, 1794 (2013).
[5]V. Ryzhii, T. Otsuji, M. Ryzhii, V. G. Leiman, S. O. Yurchenko, V. Mitin, and M. S. Shur, J. Appl. Phys. **112**, 104507 (2012).
[6]V. Ryzhii, M. Ryzhii, V. Mitin, M. S. Shur, A. Satou, and T. Otsuji, J. Appl. Phys. **113**, 174506 (2013).
[7]V. Ryzhii, A. A. Dubinov, V. Ya. Aleshkin, M. Ryzhii, and T. Otsuji, Appl. Phys. Lett. **103**, 163507 (2013).
[8]V. Ryzhii, A. A. Dubinov, T. Otsuji, V. Ya. Aleshkin, M. Ryzhii, and M. S. Shur, Opt. Express **21**, 31567 (2013).
[9]V. Ryzhii, M. Ryzhii, and T. Otsuji, J. Appl. Phys. **101**, 083114 (2007).
[10]F. Rana, IEEE Trans. Nanotechnol. **7**, 91 (2008).
[11]A. A. Dubinov, V. Ya. Aleshkin, M. Ryzhii, T. Otsuji, and V. Ryzhii, Appl. Phys. Express **2**, 092301 (2009).
[12]V. Ryzhii, M. Ryzhii, A. Satou, T. Otsuji, A. A. Dubinov, and V. Ya. Aleshkin, J. Appl. Phys. **106**, 084507 (2009).
[13]V. Ryzhii, A. A. Dubinov, T. Otsuji, V. Mitin, and M. S. Shur, J. Appl. Phys. **107**, 054505 (2010).
[14]V. Ryzhii, M. Ryzhii, V. Mitin, and T. Otsuji, J. Appl. Phys. **110**, 094503 (2011).
[15]S. Boubanga-Tombet, S. Chan, T. Watanabe, A. Satou, V. Ryzhii, and T. Otsuji, Phys. Rev. B **85**, 035443 (2012).
[16]T. Watanabe, T. Fukushima, Y. Yabe, S. A. Boubanga-Tombet, A. Satou, A. A. Dubinov, V. Ya. Aleshkin, V. Mitin, V. Ryzhii, and T. Otsuji, New. J. Phys. **15**, 075003 (2013).
[17]T. Otsuji, S. A. Boubanga Tombet, A. Satou, M. Ryzhii, and V. Ryzhii, IEEE J. Sel. Top. Quantum Electron. **19**, 8400209 (2013).
[18]A. Tredicucci and M. S. Vitiello, IEEE J. Sel. Top. Quantum Electron. **20**, 8500109 (2014).
[19]R. M. Feenstra, D. Jena, and G. Gu, J. Appl. Phys **111**, 043711 (2012).
[20]F. T. Vasko, Phys. Rev. B **87**, 075424 (2013).
[21]V. Ryzhii, T. Otsuji, M. Ryzhii, and M. S. Shur, J. Phys. D: Appl. Phys. **45**, 302001 (2012).
[22]V. Ryzhii, A. Satou, T. Otsuji, M. Ryzhii, V. Mitin, and M. S. Shur, J. Phys. D: Appl. Phys. **46**, 315107 (2013).
[23]F. Vasko and V. Ryzhii, Phys. Rev. B **77**, 195433 (2008).
[24]V. Ryzhii and M. Ryzhii, Phys. Rev. B **79**, 245311 (2009).
[25]V. Ryzhii, M. Ryzhii, N. Ryabova, V. Mitin, and T. Otsuji, Jpn. J. Appl. Phys., Part 1 **48**, 04C144 (2009).
[26]F. Xia, T. Murller, Y.-M. Lin, A. Valdes-Garsia, and F. Avouris, Nat. Nanotechnol. **4**, 839 (2009).
[27]V. Ryzhi, M. Ryzhii, V. Mitin, and T. Otsuji, J. Appl. Phys. **107**, 054512 (2010).
[28]T. Mueller, F. Xia, and Ph. Avouris, Nat. Photonics **4**, 297 (2010).
[29]M. C. Lemme, F. H. L. Koppens, A. L. Falk, M. S. Rudner, H. Park, L. S. Levitov, and C. M. Marcus, Nano Lett. **11**, 4134 (2011).
[30]V. Ryzhii, N. Ryabova, M. Ryzhii, N. V. Baryshnikov, V. E. Karasik, V. Mitin, and T. Otsuji, Opto-Electron. Rev. **20**, 15 (2012).
[31]M. Freitag, T. Low, and Ph. Avouris, Nano Lett. **4**, 1644 (2013).
[32]S. Song, Q. Chen, L. Jina, and F. Suna, Nanoscale **5**, 9615 (2013).
[33]K. S. Novoselov, V. I. Falko, L. Colombo, P. R. Gellert, M. G. Schwab, and K. Kim, Nature **490**, 192 (2012).
[34]H. C. Liu, H. Luo, D. Ban, M. Wchter, C. Y. Song, Z. R. Wasilewski, M. Buchanan, G. C. Aers, A. J. SpringThorpe, J. C. Cao, S. L. Feng, B. S. Williams, and Q. Hu, Proc. SPIE **6029**, 602901 (2005).
[35]V. Ryzhii, I. Khmyrova, M. Ryzhii, and V. Mitin, Semicond. Sci. Technol. **19**, 8 (2004).
[36]A. Shik, *Quantum Wells: Physics and Electronics of Two-Dimensional Systems* (World Scientific, London, 1998).
[37]F. T. Vasko and A. V. Kuznetsov, *Electronic States and Optical Transitions in Semiconductor Heterostructures* (Springer, New York, 1999).
[38]A. A. Dubinov, V. Ya. Aleshkin, V. Ryzhii, M. S. Shur, and T. Otsuji, J. Appl. Phys. **115**, 044511 (2014).
[39]F. Luc, E. Rosencher, and Ph. Bois, Appl. Phys. Lett. **62**, 2542 (1993).
[40]V. V. Popov, O. V. Polischuk, S. A. Nikitov, V. Ryzhii, T. Otsuji, and M. S. Shur, J. Opt. **15**, 114009 (2013).